Alloy Corrosion

R.C. Newman, S.G. Corcoran, J. Erlebacher, M.J. Aziz, and K. Sieradzki

Introduction

The corrosion properties of alloys are of enormous practical importance: modern life would be very different without stainless steels. Alloy corrosion is also an intriguing field of scientific study that combines electrochemical kinetics with fashionable aspects of the morphological evolution of surfaces and even a dash of ancient history, via the studies of Forty[1] and Lechtman[2] on "depletion gilding" practiced by Early Andeans during pre-Columbian times in South America.

The basic alloy corrosion process, as used by the metalsmiths to gold-coat artifacts, is *de-alloying*. This is defined as the selective electrolytic dissolution of one or more components from a metallic solid solution. For this to happen, there must be a significant difference in the equilibrium metal/metal-ion electrode potentials for the two metals, taking into account any complex ions that might be formed in the electrolyte. For example, we can expect de-alloying in Au-Cu alloys, but not in Au-Pt alloys.

De-alloying shows sharp *parting limits*, expressed as critical atom percentages of the more reactive component above which that component can be removed from the alloy by electrochemical dissolution in an oxidizing environment such as nitric acid. Parting limits range from about 20 at.% to 60 at.%. This concept is still used in noble metal technology to separate noble metals from base metals. For example, an alloy of 55 at.% gold and 45 at.% silver does not de-alloy, but if it is re-melted with additional silver so that the atom fraction of Ag is greater than 60%, the gold can be separated almost completely by nitric acid immersion.

De-alloying was actively used as an investigatory tool in the study of physical metallurgy around 1920, notably by Tammann[3] and by Masing.[4] Tammann proposed a model based on patterns formed by the elements in an ordered alloy and misinterpreted the existence of sharp parting limits as evidence for such ordering. Masing, on the other hand, adopted what would now be called a percolation approach, based on an attempt to calculate the probability of a continuous filament of active atoms in a random solid-solution alloy (we discovered Masing's work only recently).

Clearly it is not sufficient for an alloy to contain a continuous "filament" of reactive atoms if the filament is too narrow to admit water or ions into the resulting channel. De-alloying must involve surface diffusion of the more noble component(s) in order to open up the channels for water ingress. Forty[5–9] showed beautiful transmission-electron-microscopy (TEM) pictures of de-alloying in Au-Ag alloys, illustrating how the surface diffusion of gold opened up channels and formed bicontinuous structures similar to the morphology seen in vapor deposition of metals such as gold on glass.

Percolation and Alloy Corrosion

In alloy systems where the ambient temperature corresponds to a small fraction of the homologous melting temperature, site-percolation thresholds set a lower bound on the parting limit, or what we have termed the de-alloying threshold. In this case, de-alloyed microstructures are bicontinuous, as shown in Figure 1. Nearest-neighbor connected paths of the more electrochemically active element provide quenched-in atomic-scale paths for electrolyte penetration into the solid. As the less noble metal is selectively leached from the solid, the de-alloyed morphology undergoes coarsening. In all but a few alloy systems, the parting limit is greater than the percolation threshold because there is not a large enough difference between the equilibrium metal/metal-ion electrode potentials of the metals comprising the alloy; that is, the overvoltage that can be applied for selective dissolution is limited. The parting limit represents the critical content of reactive alloy component that is required to allow de-alloying at an arbitrarily high anodic potential. However, as shown in Figure 2, any alloy, even one that greatly exceeds the parting limit, does not show de-alloying (or rather, macro-de-alloying) below a certain potential known as the *critical potential*. Sieradzki[10] presented a model of the critical potential, building on earlier computer simulations, in which the roughening action of selective dissolution was balanced by the smoothening action of surface diffusion.[11] Later, we show advanced simulations of this process, displaying very good agreement with experimental data.

Another field of alloy corrosion in which sharp compositional threshold behavior is observed is *passivation*. To the corrosion scientist, this term means the

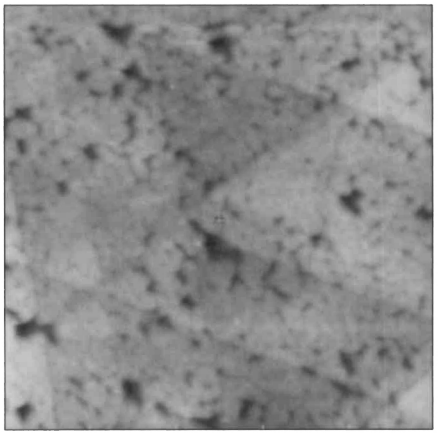

Figure 1. A 250 nm × 250 nm scanning-tunneling-microscopy (STM) image of the resultant surface morphology of a $Ag_{0.71}Au_{0.29}$ alloy after selective dissolution of Ag in 0.1 M $HClO_4$.

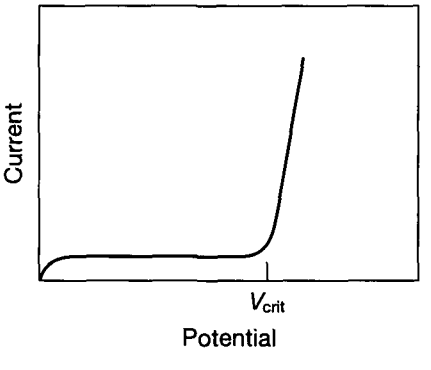

Figure 2. Schematic diagram showing typical current-voltage (potential) behavior of an alloy above the parting limit. At potentials below the critical potential V_{crit}, the current is independent of the voltage indicative of a transport-limited process. Bulk de-alloying does not occur at potentials less than the critical potential.

formation of a thin, protective oxide film, despite considerable anodic overpotential serving as a driving force for metal dissolution. Iron is very difficult to passivate in an acid solution such as sulfuric acid, but if it is alloyed with a small amount of chromium, the alloy passivates in a manner similar to pure chromium. Careful experiments on sputtered thin films of Fe-Cr alloys[12] showed that extremely sharp thresholds in passivation behavior were present at atomic percentages of Cr corresponding to percolation thresholds (10 at.% and 17 at.% for interactions up to third and second nearest neighbors, respectively) for formation of an infinitely connected three-dimensional oxide network by Cr-O-Cr polymerization. These thresholds apply to a bare metal surface that is trying to passivate. If the metal already carries its natural air-formed oxide film, then the ability of this film to survive immersion in a corrosive environment such as salt water shows an extremely sharp threshold at 13 at.% Cr. This is the threshold that drove the historical development of stainless steels, and it still defines the permitted composition ranges for several industrial alloys (although interestingly, these are often allowed to have as little as 12 at.% Cr).

Even though various aspects of alloy corrosion have been studied for the past 80 years, remarkably little detailed experimental data are available over a complete alloy-composition range. Over the past few years, Newman's group and Sieradzki's group have focused on developing experimental data for the Ag-Au alloy system, which displays complete solid solubility. Detailed experiments have been performed, aimed at measuring the critical potential as a function of alloy composition, electrolyte composition, and temperature. *In situ* scanning tunneling microscopy (STM) and *in situ* small-angle neutron scattering (SANS) are being used to characterize the morphological evolution of de-alloyed microstructures. In what follows, we summarize our results for the critical potential as well as our *in situ* SANS measurements.

The Critical Potential

Consider de-alloying in the binary system A_pB_{1-p}, which has perfect solid solubility across the composition range, where B is the more noble component and p is the atom fraction of A in the alloy. Assume that the voltage (electrochemical potential) is set at a value where component A dissolves and component B does not. If p is greater than the site-percolation threshold, there are quenched-in, nearest-neighbor connected pathways for the electrolyte to follow into the solid. In this case, transport of component A to the surface by volume diffusion is not necessary for de-alloying. Dissolution of component A results in the development of atomic-scale surface roughening. The resultant curvature sets up a gradient in the chemical potential of atoms on the surface, driving surface diffusion and a surface smoothening process. Thus de-alloying can be viewed as a competition between selective dissolution, which roughens the surface, and surface diffusion, which smoothens the surface. The length scale ξ, associated with dissolution-induced roughening, is determined by the diameter of the percolation backbone, which is a function of the alloy composition and, in a mean-field approach, assumes a value equal to $(1 + p)a/(1 - p)$, where a is the nearest-neighbor distance. These physical arguments can be put into a mathematical form that results in a fourth-order, nonlinear, partial differential equation.[10] The solution of the linearized version of this equation gives a critical dissolution flux above which dissolution-induced roughening outruns smoothening by surface diffusion at length scales greater than or equal to ξ. This critical dissolution flux can be cast into a critical potential using the Butler-Volmer equation, which is the constitutive relation between current density and electrochemical potential. The final result for the critical potential V_{crit} takes the form[10]

$$V_{crit} = 4\frac{\gamma\Omega}{nqa}\left(\frac{p}{2-p}\right) + \frac{2k_BT}{nq}\sinh^{-1}\left[\frac{32\pi^2N_sD_s}{a^2J_0}\left(\frac{p}{2-p}\right)^2\right]. \quad (1)$$

In this equation, γ is the solid/electrolyte interfacial free energy, Ω is the atomic volume, n is the number of electrons transferred in the dissolution reaction, q is the elementary charge of an electron, k_B is Boltzmann's constant, T is the absolute temperature, N_s is the surface density of atoms, D_s is the surface diffusivity, and J_0 is the mass flux corresponding to the exchange-current density. The exchange-current density corresponds to the forward or backward steady-state mass flux of ions at the equilibrium potential and is a function of the electrolyte composition. The unknown parameters in this equation are γ, D_s, and J_0, and in principle, each of these quantities may be determined independently in separate experiments. All three parameters depend on the alloy composition and the composition of the electrolyte (the concentration of dissolved Ag^+, in the case considered next).

Figure 3 shows results recently obtained at 25°C by Sieradzki's group for the critical potential of Ag-Au alloys in 1 M $HClO_4$ containing various concentrations of Ag^+ dissolved in the electrolyte.[13] We note that the J_0 parameter just discussed increases with dissolved Ag^+ concentration in the electrolyte. These results were fitted to Equation 1 for the critical potential using two adjustable constants, γ and the ratio $D_sJ_0^{-1}$. Table I

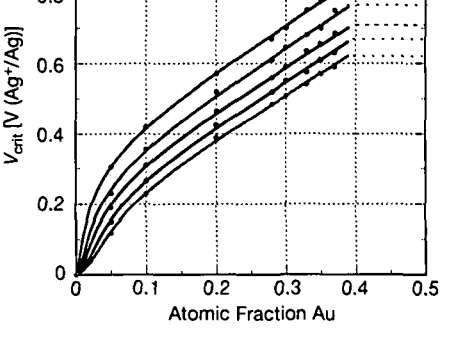

Figure 3. Experimentally determined values (data points) of the critical potential of Ag-Au alloys in 0.1 M $HClO_4$ + Ag^+ as a function of the Au concentration in at.%. The solid curves through the data are the theoretical fits using Equation 1 for V_{crit}. Curves in ascending order correspond to Ag^+ electrolyte concentrations of 1, 0.1, 0.01, 0.001, and 10^{-4} M. Fitting parameters are shown in Table I. V_{crit} is measured with respect to the 0.1 M $HClO_4$ + Ag^+/Ag reference electrode.

Table I. Parameters used to fit the theoretical equation for the critical potential to the experimental data shown in Figure 3.

$[Ag^+]$ [M]	γ [J m^{-2}]	$D_sJ_0^{-1}$ [cm^4]	D_s [cm^2 s^{-1}]
0.0001	0.93	1.63×10^{-28}	
0.001	0.90	5.31×10^{-29}	5×10^{-11}
0.01	0.87	2.35×10^{-29}	
0.1	0.84	1.17×10^{-29}	3×10^{-10}
1	0.81	5.71×10^{-30}	

shows the results for these parameters as a function of the Ag^+ concentration in the electrolyte. We were able to determine D_s (see Table I) by using some known data[14] for the exchange-current density at Ag^+ concentrations of 10^{-3} M and 10^{-1} M. The values of γ and D_s in Table I are consistent with those obtained from other measurements of D_s and first-principles calculations of γ for Au(111) surfaces.[15,16] These experimental results provide an important validation of our understanding of de-alloying.

In Situ SANS

Corcoran et al.[17,18] have used SANS to study the kinetic processes associated with coarsening of de-alloyed microstructures. These experiments were performed using the 30-m-long SANS instrument at the National Institute of Standards and Technology Center for Neutron Research. The neutron beam was pinhole-collimated. A beam wavelength of 6 Å was used. The measurement range for the scattering vector **Q** was 0.003–0.11 $Å^{-1}$.

Samples prepared from a $Ag_{0.7}Au_{0.3}$ alloy were placed vertically in a quartz electrochemical cell.[22] An electrolyte of 1 M $HClO_4$ + 1 mM Ag^+ was circulated through the cell from a 500-ml reservoir. A silver wire reference electrode was used. All potentials in this section are referenced to the Ag/Ag^+ equlibrium potential and hence represent an overpotential for elemental Ag dissolution.

SANS data were recorded over a period of 39 h. The sample was de-alloyed at 700 mV for 19 h, followed by holding the potential at 450 mV for 20 h. Figures 4 and 5 show representative data over this 39-h period. Only a small increase in the scattering intensity was observed during the 19 h of de-alloying at 700 mV, as shown in Figure 4. A preferential increase in the scattering intensity is observed at a **Q** value of approximately 0.030 $Å^{-1}$. However, not until the potential was decreased below the de-alloying potential (to 450 mV) did the scattering intensity increase substantially. In Figure 4, the first data taken after only 10 min at 450 mV display a substantially increased scattering intensity and the development of a well-defined peak at a **Q** value of approximately 0.032 $Å^{-1}$.

The formation of a peak corresponds to the development of a well-defined length scale in the de-alloyed microstructure, that is, the formation of a well-defined average "pore size." Owing to the inverse relationship between scattering vector **Q** and real space length scales, we see a decrease in the scattering intensity at large **Q** as a result of a decrease in the total volume of the smallest pores in the structure. This decrease is a result of ambient temperature coarsening.

Figure 5 shows the scattering data during the 20-h hold at 450 mV. The porosity continues to coarsen with time as evidenced by the continual shifting of the peak position to smaller values of **Q**. After 20 h at 450 mV, the peak position shifted from approximately 0.032 $Å^{-1}$ to 0.017 $Å^{-1}$. If we take the average pore size to be proportional to the inverse of the peak position, we calculate a doubling of the average pore size during this 20-h period.

What was most surprising about these results is that no significant coarsening is observed at the 700-mV de-alloying potential. The size scale of the porosity appears to be quenched-in. This suggests that a surface layer has formed on the gold, resulting in a dramatic decrease in the surface diffusivity. One possible explanation is that gold oxidation has begun. The potential of 700 mV corresponds to a potential just prior to the first stages of gold oxidation, namely, hydroxide formation.[19–21] The formation of gold hydroxide may be inhibiting the coarsening of the porous structure. We are currently trying to confirm the presence of Au hydroxide at this potential.

Potential-dependent coarsening behavior for porous Au was also reported by Kelly et al.,[22] using electrochemical impedance spectroscopy.

The SANS data were analyzed using the leveled wave method of Berk.[23,24] Examples of data fitted with this model can be found in our previous publications.[17,18] Figures 6a and 6b are simulated two-dimensional slices through the calculated structure for the scattering data, taken after 1.7 h and 19.7 h, respectively. The average ligament width was found by making chord-length measurements through the image. The average ligament width was found to be 7.8 nm after 1.7 h of coarsening and 15.0 nm after 19.7 h of coarsening.

Figure 7 shows the results for the average ligament width versus time. The slope of the double-logarithmic plot is 0.28, which is between that expected for a surface-diffusion ($t^{1/4}$) and a volume-diffusion ($t^{1/3}$) process. This power-law behavior is identical to that found earlier by Kelly et al. using an impedance spectroscopy technique.[22] Further interpretation of these data requires that we take into account the fact that the scattering is averaged over the thickness of the sample; that is, some porosity has been exposed to the electrolyte for longer periods of time than others. By correcting the aver-

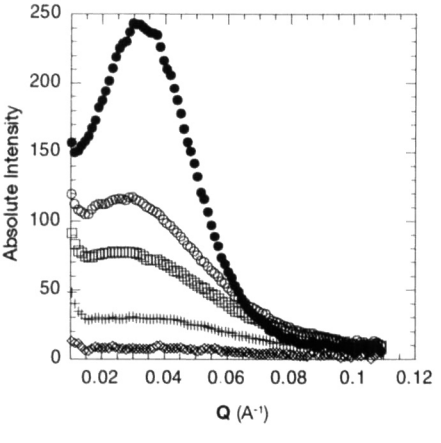

Figure 4. In situ *small-angle-neutron-scattering (SANS) data for the potentiostatically controlled corrosion of $Ag_{0.7}Au_{0.3}$ obtained at 700 mV (Ag/10^{-3} M Ag^+). Curves in ascending order correspond to times of 2.9, 7.3, 12.5, and 18.7 h, respectively. After 18.7 h, the potential was decreased to 450 mV, which was below the de-alloying potential. The last curve was obtained 10 min after the potential was decreased to 450 mV.*

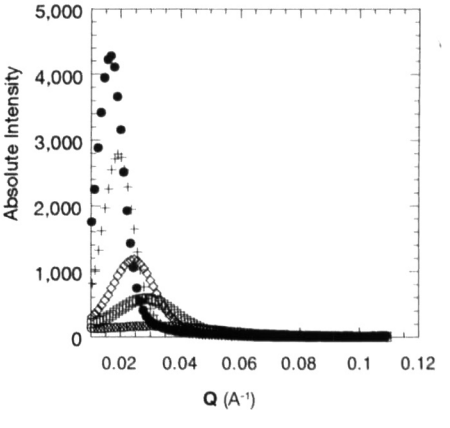

Figure 5. In situ *SANS data for the potentiostatically controlled corrosion of $Ag_{0.7}Au_{0.3}$. The sample was de-alloyed at 700 mV (versus Ag/10^{-3} M Ag^+) for 18.7 h. The potential was then decreased below the de-alloying potential to 450 mV, and the scattering data were recorded. Curves in ascending order correspond to times of 0.1, 1.7, 3.9, 10.9, and 20.1 h at 450 mV.*

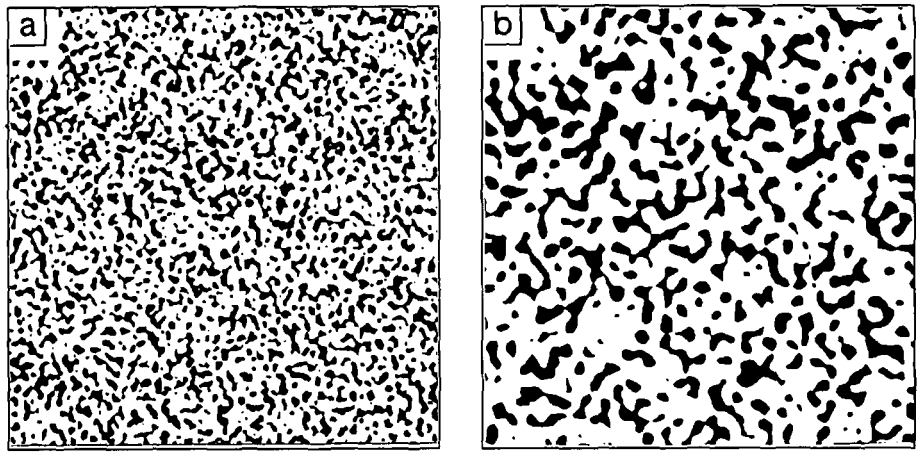

Figure 6. Simulated transmission-electron-microscopy images (768 nm × 768 nm) calculated from fits to the scattering data for (a) 1.7 h and (b) 19.7 h at 450 mV. The average ligament width calculated from the images is (a) 7.8 nm and (b) 15.0 nm.

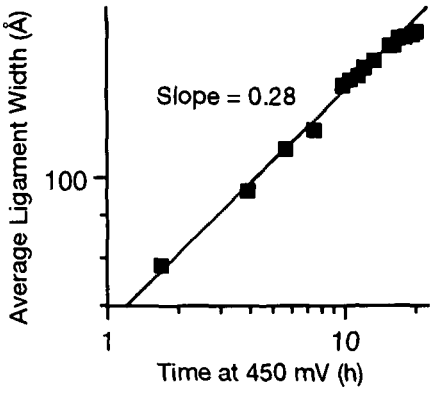

Figure 7. Double-logarithmic plot of the average ligament width versus time at 450 mV. The slope is 0.28.

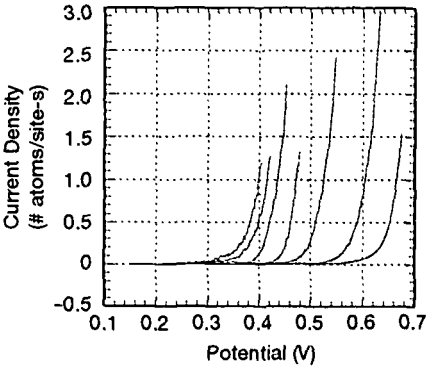

Figure 8. Kinetic Monte Carlo (KMC) results showing the current density versus potential behavior of Ag-Au alloys. The potential (voltage) is measured with respect to the potential of elemental Ag dissolution. The curves in the figure (left to right) correspond to alloy compositions of 5, 10, 15, 17.5, 20, 30, and 40 at.% gold.

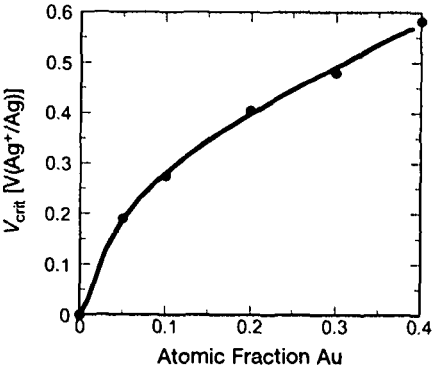

Figure 9. KMC results (•) of the critical potential found for Ag-Au alloys versus at.% Au. The solid line is a fit based on the continuum model of critical potential. Compare these results to those of Figure 3.

age ligament width versus time for this averaging, we should be able to obtain more conclusive data on the dominant transport mechanism involved in the coarsening process.

Computer Simulations

In order to examine some critical issues connected with kinetics, Erlebacher et al. have been performing Kinetic Monte Carlo (KMC) simulations of alloy corrosion processes.[25] The approach is to identify the simplest atomic-scale picture capable of showing behavior paralleling the key experimental results that we have described here. In particular, a realistic simulation should be able to show the appropriate current-voltage behavior, including a critical potential, a de-alloying threshold, a bicontinuous de-alloyed microstructure, and coarsening kinetics.

The advantage of the KMC approach is that the simulations incorporate real-time kinetics that are obtained from experimental rate laws. Additionally, these simulations are fully three-dimensional, multicomponent, and model the real crystallography of the structure. Bond energies, adatom surface diffusivities, and elemental dissolution rates serve as inputs to the model. Figure 8 shows some of our results from KMC simulations for the current density versus potential behavior of Ag-Au alloys. This is the first time that critical potential behavior has been observed in computer simulations of alloy corrosion. Figure 9 demonstrates that the critical potential behavior found in the simulations parallels that observed in experiment. The KMC simulations also show coarsening behavior that scales as $t^{1/4}$. We are in the process of performing a detailed analysis comparing simulated and experimental results.[25]

Summary and Conclusions

Figure 3 shows a parting limit, or de-alloying threshold, at the alloy composition $Ag_{0.6}Au_{0.4}$; that is, for alloys containing less than 60 at.% Ag, macroscopic de-alloying does not occur. In face-centered-cubic (fcc) solids, the site-percolation threshold occurs at approximately 20 at.% Ag, and so a natural question to consider is, "Why is Ag inaccessible to the electrolyte in the intervening composition range?" One explanation for this is that in the composition range 20–60 at.% Ag, the channels that open are too narrow to permit penetration of the electrolyte. In this case, the following physical picture emerges. As the silver concentration in the alloy is reduced, the mean diameter of the percolation backbone decreases, and so the driving force (voltage) necessary for silver removal increases. As long as the gold atoms remaining at the bottom of these channels have some minimum surface mobility, selective dissolution to significant depths (macroscopic de-alloying) is possible. However, there is a limit to the voltage that can be applied for silver removal while retaining gold mobility, and this limit is connected with gold hydroxide or oxide formation. For alloy concentrations less than about 60 at.% Ag, the large overvoltage required for selective dissolution of silver also results in simultaneous gold oxidation. Thus electrolyte penetration into the de-alloyed channels

becomes limited, and bulk macroscopic de-alloying cannot occur. The SANS results showing the morphological evolution of the de-alloyed microstructure for a $Ag_{0.7}Au_{0.3}$ alloy support the notion that, at high potentials, the surface mobility of gold is greatly reduced. Apparently, in the case of the $Ag_{0.7}Au_{0.3}$ alloy, the diameter of the percolation backbone is large enough to permit electrolyte penetration and de-alloying, even at the high potentials that result in gold oxidation.

Figure 4 showing data taken at 700 mV indicates a microstructure that is virtually quenched-in. Shifting the potential to 450 mV almost immediately results in significantly increased coarsening kinetics.

The KMC simulations are helping us to sort out the issues described above, and future simulations will examine the more difficult problem of the compositional dependence of passivation in the FeCr system.

Acknowledgments

M.J. Aziz and K. Sieradzki gratefully acknowledge support of this work under separate U.S. Department of Energy, Division of Materials Sciences, Office of Basic Energy Sciences grants DE-FG02-89ER45401 and DE-FG03-94ER45224, respectively.

References

1. A.J. Forty, *Nature* **282** (1979) p. 597.
2. H. Lechtman, *Sci. Am.* **250** (1984) p. 56.
3. G. Tammann, Z. *Anorg. Chem.* **107** (1919) p. 9; *ibid.* **112** (1920) p. 233; *ibid.* **114** (1920) p. 281.
4. G. Masing, *ibid.* **118** (1921) p. 293.
5. A.J. Forty, *Gold Bull.* **14** (1981) p. 25.
6. A.J. Forty and P. Durkin, *Philos. Mag. A* **42** (1980) p. 295.
7. A.J. Forty and G. Rowlands, *ibid.* **43** (1981) p. 171.
8. P. Durkin and A.J. Forty, *ibid.* **45** (1982) p. 95.
9. A.J. Forty, in *Sir Charles Frank, an Eightieth Birthday Tribute*, edited by R. Chambers, J. Enderby, A. Keller, A. Lang, and J. Steeds (Adam Hilger, Bristol, 1991) p. 164.
10. K. Sieradzki, *J. Electrochem. Soc.* **140** (1993) p. 2868.
11. K. Sieradzki, R.R. Corderman, K. Shukla, and R.C. Newman, *Philos. Mag. A* **59** (1989) p. 713.
12. S. Fujimoto, G.S. Smith, R.C. Newman, S.P. Kaye, H. Kheyrandish, and J.S. Colligon, *Corros. Sci.* **35** (1993) p. 51.
13. K. Sieradzki, D. Movrin, C. McCall, and N. Dimitrov (unpublished).
14. K.J. Vetter, *Electrochemical Kinetics* (Academic Press, New York, 1967) p. 668.
15. I.C. Oppenheim, D.J. Trevor, C.E.D. Chidsey, P.L. Trevor, and K. Sieradzki, *Science* **254** (1991) p. 687.
16. R.C. Cammarata and K. Sieradzki, *Ann. Rev. Mater. Sci.* **24** (1994) p. 215.
17. S.G. Corcoran, D.G. Wiesler, J. Barker, and K. Sieradzki, in *Neutron Scattering in Materials Science II*, edited by D.A. Neumann, T.P. Russell, and B.J. Wuensch (Mater. Res. Soc. Symp. Proc. **376**, Pittsburgh, 1995) p. 377.
18. S.G. Corcoran, D.G. Wiesler, and K. Sieradzki, in *Electrochemical Synthesis and Modification of Materials*, edited by P.C. Andricacos, S.G. Corcoran, J.-L. Delplancke, T.P. Moffat, and P.C. Searson (Mater. Res. Soc. Symp. Proc. **451**, Pittsburgh, 1997) p. 93.
19. H. Angerstein-Kozlowska, B.E. Conway, A. Hamelin, and L. Stoicoviciu, *J. Electroanal. Chem.* **228** (1987) p. 429.
20. Z. Jusys and S. Bruckenstein, *Electrochem. Solid-State Lett.* **1** (1998) p. 74.
21. S.G. Corcoran, PhD thesis, The Johns Hopkins University, 1994.
22. R.G. Kelly, A.J. Young, and R.C. Newman, in *ASTM STP 1188: Electrochemical Impedance: Analysis and Interpretation*, edited by J.R. Scully, D.C. Silverman, and M.W. Kendig (American Society for Testing and Materials, Philadelphia, 1993) p. 94.
23. N.F. Berk, *Phys. Rev. Lett.* **58** (1987) p. 2718.
24. N.F. Berk, *Phys. Rev. A* **44** (1991) p. 5069.
25. J. Erlebacher, K. Sieradzki, and M.J. Aziz, in preparation. □